J Mater Sci (2018) 53:4598–4611

Metals

Atomic scale HAADF-STEM study of η' and η_1 phases in peak-aged Al–Zn–Mg alloys

Artenis Bendo[1,*], Kenji Matsuda[2], Seungwon Lee[2], Katsuhiko Nishimura[2], Norio Nunomura[3], Hiroyuki Toda[4], Masatake Yamaguchi[5], Tomohito Tsuru[5], Kyosuke Hirayama[4], Kazuyuki Shimizu[4], Hongye Gao[4], Kenichi Ebihara[5], Mitsuhiro Itakura[5], Tomoo Yoshida[6], and Satoshi Murakami[6]

[1] *Graduate School of Science and Engineering for Education, University of Toyama, Toyama, Japan*
[2] *Graduate School of Science and Engineering for Research, University of Toyama, Toyama, Japan*
[3] *Information Technology Center, University of Toyama, Toyama, Japan*
[4] *Department of Mechanical Engineering, Kyushu University, Fukuoka, Japan*
[5] *Japan Atomic Energy Agency, Tokai, Japan*
[6] *Aisin Keikinzoku Co., Ltd., Kariya, Japan*

Received: 30 September 2017
Accepted: 27 November 2017
Published online: 11 December 2017

ABSTRACT

The microstructures of precipitates in Al–Zn–Mg alloys in peak-aged condition have been studied using scanning transmission electron microscope. The same thermo-mechanical treatment was applied in all alloys. Investigation of peak-aged samples revealed that the most commonly found phases were η' and η_1 with their respective habit planes on $\{111\}_{Al}$ and $\{100\}_{Al}$. η' phases under $[110]_{Al}$ were analyzed and compared with η' structure models. Furthermore, a close inspection of η_1 phase as the second most found precipitate revealed that it incorporates an anti-phase resembling boundary, not observed in other orientation relationships that precipitates create with Al matrix, in addition, differences in matrix-precipitate interfaces between η'/η_2 and η_1 phases were noticed. This paper addresses the first part to the analysis of η' phase. Next part is extended to the analysis of the η_1 phase.

Introduction

Al–Zn–Mg alloys because of their age-hardenable potential can attain high specific strengths by the homogeneous dispersion of fine precipitates formed during aging heat treatment [1]. Al–Zn–Mg alloys decompose during aging at low temperatures after a rapid quench from solid solution temperatures via formation of GPI and GPII zones [2]. GP-zones named after Guinier and Preston are well known that appear in Al alloys during initial stages of aging at low temperatures as zones rich in solute atoms and coherent with matrix [3]. GPI-zones were detected using electron diffractions as diffuse spots near forbidden diffraction spots from {100} sets of Al planes in vast majority of Al alloys. An general atomic model was proposed which explains diffraction spots associated with these zones in selected area

Address correspondence to E-mail: ikenolab@eng.u-toyama.ac.jp

https://doi.org/10.1007/s10853-017-1873-0

diffraction patterns (SADPs) based on substitution of solute atoms in a short-range order and anti-phase boundary structure [4]. GPII zones were reported as Zn-rich, plate-like, few atomic layers thick and 3–6 nm wide lying on the same habit plane as η' phase. They nucleate heterogeneously in vacancy-rich solute clusters (VRC) that have aggregated on $\{111\}_{Al}$ planes. GPII zones have internal order in form of elongated Zn-rich layers substituting $\{110\}_{Al}$ planes. Their diffraction spots appear near positions of η' phase diffraction spots from $\{11\bar{2}0\}_{\eta'}$ set of planes. Their characteristic electron diffraction pattern is also seen in Al–Zn alloys, which confirms that these zones are heavily enriched in Zn atoms [2, 5]. Both these early stage aging precipitates are thought as precursors of the η' phase [6–8]. Peak hardness of Al–Zn–Mg alloys is attributed to the fine scale precipitation of the metastable η' phase [9]. Researchers have reported lattice parameters for this metastable hexagonal phase throughout years as shown in Table 1. The generally agreed lattice parameter for η' phase is $a = 0.496$ nm and $c = 1.405$ nm to make it fully coherent with Al matrix [10–19]. Proposed η' crystal structures models are that of Gjonnes [12], Auld [14], Li [18] and Kverneland [19]. Recently, two new structure models were built upon HAADF images of the common precipitates found in peak strength condition [20]. These peak-aged precipitate structures stand very near to the structural pattern of the η equilibrium phase structure [20, 21]. In addition, equilibrium η phase can appear with nine different orientation relationships with the Al matrix, named η_1–η_9 [12]. The dominating precipitated orientation relationship of η phase with the matrix depends on which decomposition mechanisms will predominate the aging process [22–24]. Ageing above 200 °C, T phase, $(AlZn)_{49}Mg_{32}$ will be readily nucleated [25, 26]. Previous researchers refer to T phase as X-phase [24, 27, 28]. Cu is usually added to 7xxx Al series to increase the rate of age-hardening during initial stages of aging and strength during later stages. It is incorporated progressively in precipitates substituting Zn atoms, till a stable value of its content is reached. Cu incorporation into precipitates gets higher in higher Cu content alloys and higher aging temperatures. It increases GP-zone solvus temperature and stabilizes GPI-zones by coarsening them. Therefore, these coarse GPzones will resist and continue to grow during ageing because their surface energy will be lower. Small additions do not change the precipitation sequence. [4, 6, 7, 29–31, 49]. Ag addition causes refinement of precipitates by promoting early clustering of Ag and Zn atoms [30]. A lot of research has been done in characterization of η' and η_2 precipitates as the successive phases of the decomposition mechanism: supersaturated solid solution (SSSS) → GP(I, II) → η' → η_2 that brings about the highest strength when metastable η' phase forms in highest volume fraction. Furthermore, considerable controversy exists on the structure of η' phase as it is seen by many proposed structure models.

In this article the precipitates observed in our alloys peak-aged at 150 °C were studied using scanning transmission electron microscope. First part addresses to the analysis of HAADF images of η' phases taken under $[110]_{Al}$, and the next part is dedicated to the analysis of the η_1 phase for which there is not yet done a dedicated structure characterization.

Table 1 Lattice parameters of metastable hexagonal η' phase (except Gjonnes model which has a monoclinic unit cell with parameters, $a = b$, space group $P2_1$, $\gamma = 120°$; that is the building block of a hexagonal unit cell) reported by different researchers over time: $6d\{111\}_{Al} = d(0001)_{\eta'} = 1.402$ nm; $3d\{220\}_{Al} = d(10\bar{1}0)_{\eta'} = 0.429$ nm; $3d\{224\}_{Al} = d(11\bar{2}0)_{\eta'} = 0.248$ nm

Year	η'	a (nm)	c (nm)	$d(10\bar{1}0)\eta'$	$d(11\bar{2}0)\eta'$
1956	Mondolfo et al. [10]	0.496	0.868	0.429	0.248
1957	Graf et al. [11]	0.496	1.403	0.429	0.248
1970	Gjonnes et al. [12]	$b = 0.497$	0.554	0.43	0.248
1971	Auld et al. [13]	0.489	1.374	0.423	0.244
1974	Auld et al. [14]	0.496	1.402	0.429	0.248
1976	Mondolfo et al. [15]	0.496	1.402	0.429	0.248
1982	Régnier et al. [16]	0.496	1.402	0.429	0.248
1985	Auld et al. [17]	0.496	1.402	0.429	0.248
1999	Li et al. [18]	0.496	1.402	0.429	0.248
2006	Kverneland et al. [19]	0.496	1.402	0.429	0.248

Experimental procedure

Compositions of the investigated alloys are shown in Table 2. The base alloy composition is Al-2.8%Zn-2.3%Mg-0.3%Si (at.%) and was named ZM33S in which letters Z, M and S stand, respectively, for Zn, Mg and Si. Added letters to other alloys stand, respectively, C for Cu addition and A for Ag addition. These alloys were cast in permanent steel mold. The ingot was homogenized at 470 °C for 24 h. Sheets of 1.5 mm thickness and 15 mm width were extruded. Specimens were cut from the center of extruded part, cold rolled into 1-mm-thick sheets, solution treated at 475 °C for 60 min in an air furnace and quenched into iced water. Subsequently, peak-hardness condition is produced by aging carried out at 150 °C for 1000 min in silicone oil bath. The micro-Vickers hardness measurements were done with Mitutoyo HM-101, load 100 g (0.98 N) for a holding time of 15 s. Disks with a diameter of 3 mm were punched out from peak-aged foils previously thinned to around 35 μm using mechanical and electrolytic polishing. These disks were further thinned till a hole is created through them using twin-jet electrolytic polishing method in a Tenupol 3 machine. The solution used was composed of 1/3 nitric acid (HNO_3) and 2/3 methanol (CH_3OH) kept between − 30 and − 25 °C. High-angle annular dark field STEM (HAADF-STEM) imaging was carried out using a Hitachi HD-2700D STEM operating at 200 kV. Simulations of interface and electron diffraction pattern for η_1 phase were carried out using CrystalKitX and MacTempas™ software programs.

Results

Low magnification of HAADF images

HAADF imaging was applied to investigate the precipitates formed in our alloys peak-aged at 150 °C after water quenching. Considering that precipitates formed in Al–Zn–Mg alloys are plate or rod shaped expect to the T phase which has a blocky morphology, classification of precipitates on microstructural level is easily done on their habit plane. There are nine orientation relationships that η-$MgZn_2$ can create with matrix [12, 24]. Based on previous researches, the most commonly found orientation relationships of precipitates in Al–Zn–Mg alloys are η_1, η'/η_2 and η_4 [9, 12, 22, 24, 32, 33, 45]. The possibility of other orientation relationships to form is low.

On microstructural level, (see Table 3) η_1 and η_9 cannot be distinguished because of their identical morphologies as plate-like particles lying on $\{001\}_{Al}$. The only difference is on nanostructural level where η_9 is rotated 30° on $\{110\}_{Al}$ plane.

The same difference on nanostructural level but with rotation occurring on $\{111\}_{Al}$ is between η_2 and η_3, which also are indistinguishable from the microstructural level. Moreover, η' phase has identical orientation relationship as η_2. For this reason, η' is thought as precursor of η_2 phase [12].

In contrast, η_4–η_7 are all rod-/lath-shaped precipitates. Due to their high aspect ratio (length/thickness) they can be readily discerned from plate-like shaped particles. They differ from the misorientation angle that their longest dimension (which corresponds to $[0001]_\eta$) form with $\langle 110\rangle_{Al}$ (Table 3) [12, 24].

In the present work, precipitates are imaged along $[110]_{Al}$ zone axis because two from four sets of equivalent $\{111\}_{Al}$ planes are aligned parallel with the beam as seen in the simplifying model in Fig. 1d. Therefore, the probability is higher for investigating edge-on η'/η_2 particles lying on these planes. Figure 1a–c shows the microstructures containing regions of white contrast caused by precipitates imbedded in the dark fields of Al matrices. Particles lying on $\{100\}_{Al}$ and $\{111\}_{Al}$ were observed with the highest probability that these plates correspond to η_1 and η'/η_2 phases. Based on their sizes, a possible classification is done in Fig. 1a–c.

Moreover, it is clearly seen in Fig. 1 that addition of Cu or Ag increases the number density of precipitates [34]. In Cu-added alloy, number of particles with rounded morphologies is higher than in Ag-added one. From diffraction work, Cu addition causes strong intensities from diffraction spots of GPI-zones. These spots were observed even in peak-aged condition. Therefore, the observed rounded precipitates could be GP-zones that have grown coarser due to incorporation of Cu in them [31]. It confirms once

Table 2 Chemical composition of the investigated Al–Zn–Mg alloys (in at.%)

Alloys	Zn	Mg	Si	Cu	Ag	Al
ZM33S	2.81	2.3	0.29	–	–	Bal.
ZM33SC	2.76	2.18	0.29	0.22	–	Bal.
ZM33SA	2.74	2.48	0.29	–	0.2	Bal.

Table 3 Simplified classification of precipitates formed in Al–Zn–Mg alloys based on their similarities. The most commonly found precipitates are η_1, η'/η_2, η_4 and for very overaged condition T phase [12, 23, 24, 28, 32]

	Orientation relationship	Morphology (habit plane)
η'	$(0001)_{\eta'}//(1\bar{1}\bar{1})_{Al}$; $(10\bar{1}0)_{\eta'}//(110)_{Al}$	Plate on $\{111\}_{Al}$
η_2	$(0001)_{\eta}//(1\bar{1}\bar{1})_{Al}$; $(10\bar{1}0)_{\eta}//(110)_{Al}$	Plate on $\{111\}_{Al}$
η_3	$(0001)_{\eta}//(1\bar{1}\bar{1})_{Al}$; $(11\bar{2}0)_{\eta}//(110)_{Al}$	Plate on $\{111\}_{Al}$
η_1	$(0001)_{\eta}//(110)_{Al}$; $(10\bar{1}0)_{\eta}//(001)_{Al}$	Plate on $\{001\}_{Al}$
η_9	$(0001)_{\eta}//(110)_{Al}$; $(11\bar{2}0)_{\eta}//(001)_{Al}$	Plate on $\{001\}_{Al}$
η_4	$(11\bar{2}0)_{\eta}//(1\bar{1}\bar{1})_{Al}$; $[0001]_{\eta}//[110]_{Al}$	Rod/lath on $\{111\}_{Al}$
η_5	$(11\bar{2}0)_{\eta}//(1\bar{1}\bar{1})_{Al}$; $[0001]_{\eta}$ 11° to $[110]_{Al}$	Rod/lath on $\{111\}_{Al}$
η_6	$(11\bar{2}0)_{\eta}//(1\bar{1}\bar{1})_{Al}$; $[0001]_{\eta}$ 15° to $[110]_{Al}$	Rod/lath on $\{111\}_{Al}$
η_7	$(11\bar{2}0)_{\eta}//(1\bar{1}\bar{1})_{Al}$; $[0001]_{\eta}$ 25° to $[110]_{Al}$	Rod/lath on $\{111\}_{Al}$
η_8	$(11\bar{2}0)_{\eta}//(1\bar{1}2)_{Al}$; $(0001)_{\eta}//(31\bar{1})_{Al}$	Rod/lath
T	$(100)_{T}//(111)_{Al}$; $(010)_{T}//(112)_{Al}$	Globular

more the effect of Cu in stabilization of GP-zones [4, 6, 7, 29, 30].

Ag effect in refining precipitates size is clearly observed in Fig. 1c. Diffraction spots of GPI-zones cannot be seen in case of Ag-added alloy.

High magnification of HAADF images of η' phase

High-resolution imaging of plate-shaped particles lying on $\{111\}_{Al}$ planes in alloy containing Cu (ZM33SC) and Ag (ZM33SA) under $[110]_{Al}$ has been carried out as shown in Figs. 2 and 3. Due to identical orientation relationships of η' and η_2 with the matrix, edge-on particles lying on $\{111\}_{Al}$ planes, along $[110]_{Al}$ projection, will be under zone axis of $[10\bar{1}0]_{\eta'/\eta 2}$. All particles observed are built up from dark and white contrast layers. The contrast in HAADF-STEM images is related to atomic number. Therefore, for the same linear density of atomic column, enrichment in heavy atoms can be easily identified [35]. Zn ($Z = 30$) has almost twice the atomic number than the other main alloying element Mg ($Z = 12$). Since Zn is the major alloying elements which has a high Z atomic number, confirms that bright contrast layers are rich in this element and dark ones rich in Al or Mg. Regardless, there is possibility that brighter layers to include Cu or Ag atoms. Cu or Ag increases the number densities of solute clusters and GP-zones, acting as nucleation sites for precipitates, and they are excepted to be part of these particles as it is seen by their effect on precipitate sizes and distributions in Fig. 1 [34, 36].

Layer building particles shown in Figs. 2 and 3 are labeled with letters "a" for the white contrast ones (layers enriched in heavy atoms) and "b" for the dark contrast one (layers enriched in light atoms) [37].

Edge-on particles of ZM33C alloy seen in Fig. 2a, c are 13 layers thick, with 11 internal layers and interface composed of high-Z atoms.

Precipitate in Fig. 2a is composed of "a–b" layered stacking order sequence where "a" are Zn-rich layers and "b" are Mg-rich ones [38]. The internal layers of this precipitate are in full compatibility with that of equilibrium η-$MgZn_2$. A dislocation loop surrounds the precipitate. Twelve $\{111\}_{Al}$ planes are substituted by 13 layers of precipitate. Interplanar spacing of $\{111\}_{Al}$, 0.233 nm is smaller than that of precipitation, $d_{(0004)}$-$MgZn_2$, 0.21 nm [39]. Therefore, a dislocation will relax the increased strain generated by this misfit between the matrix and precipitate planes, in the middle distance of the interface [40]. In ZM33SC, substitution of Zn with Cu is found to be favorable in η-type phases due to decreasing of formation enthalpy [41].

Precipitate in Fig. 2c is 13 layers thick, and it incorporates double stacking layers "b–b" composed from light elements. Five layers in the middle of the thickness show a slightly enhanced intensity compared to the two layers situated at both sides, indicating enrichment in heavy elements. Even though the precipitate in Fig. 2c is 13 layers thick, the internal periodic layers are not composed of "a–b" stacking sequence of η-$MgZn_2$ phase and coherency is still preserved with matrix. It confirms that particles can grow to 13 layers thick, without transforming to equilibrium phase. This is in contradiction with the proposed idea that 11 layers thick is the smallest entity that can be associated with the η phase [37].

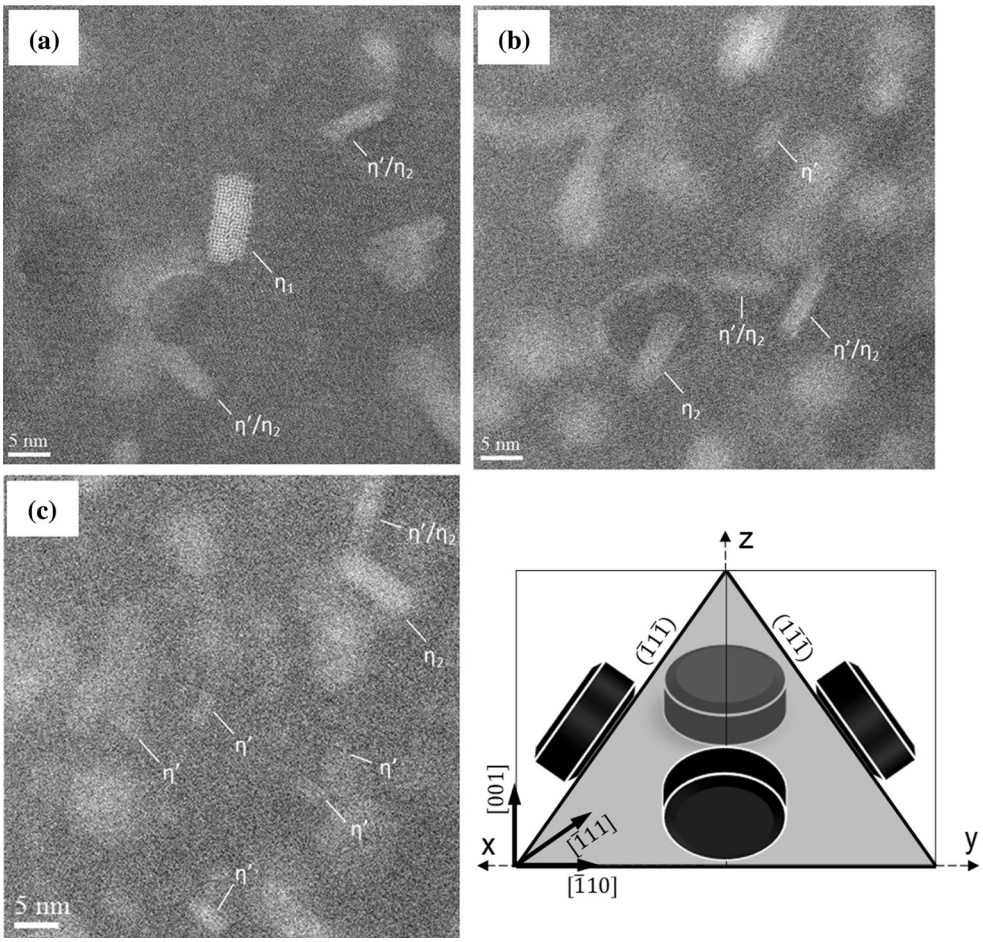

Figure 1 HAADF images of microstructures formed in alloy **a** ZM33S, **b** ZM33SC and **c** ZM33SA peak-aged at 150 °C for 1000 min under $\langle 110 \rangle_{Al}$ projection. The denotation of phases based on habit planes and aspect ratios. **d** Model of $\eta'/\eta_2/\eta_3$ precipitates morphologies lying on four equivalent $\{111\}_{Al}$ family planes under $[\bar{1}\bar{1}0]_{Al}$ projection and the corresponding diffraction axis of Al matrix.

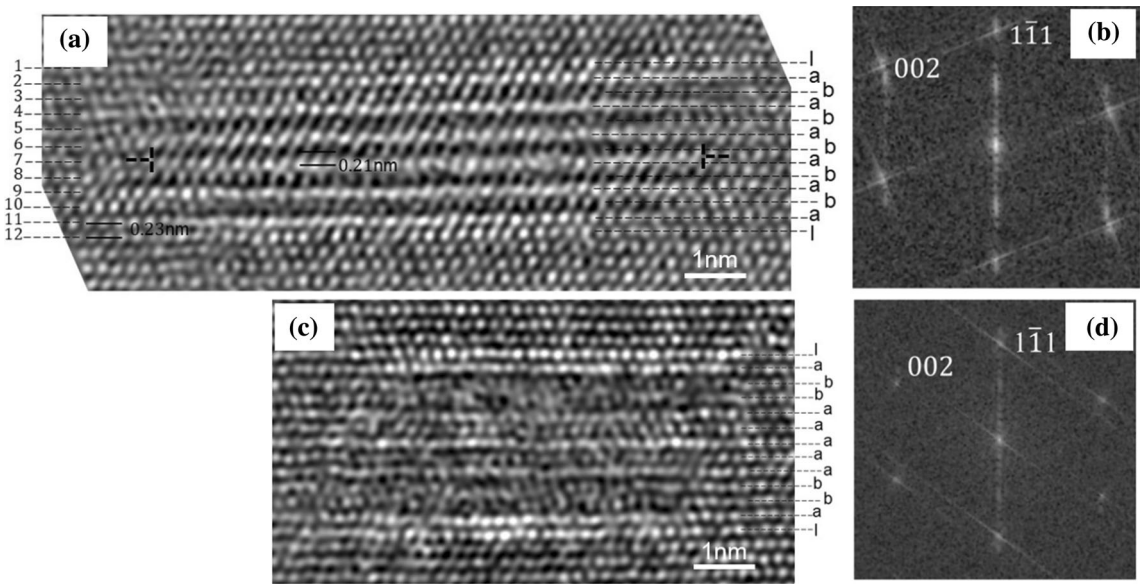

Figure 2 **a**, **c** HAADF images under $[1\bar{1}0]_{Al}$ projection of edge-on plates lying on $(1\bar{1}1)_{Al}$ planes in ZM33SC alloy peak-aged at 150 °C for 1000 min. Respective FFT processing is given in the inset (**b**) and (**d**).

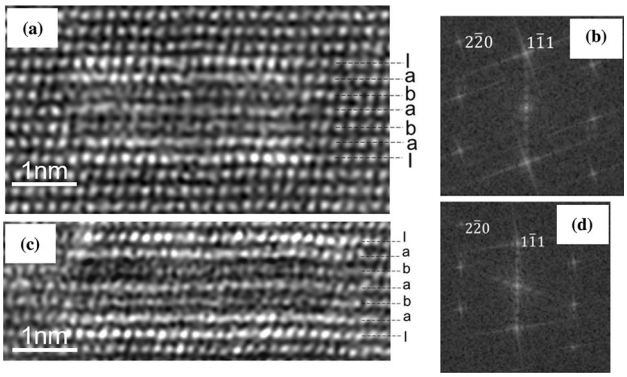

Figure 3 **a**, **c** HAADF images of edge-on precipitates lying on $(1\bar{1}1)_{Al}$ planes under $[110]_{Al}$ projection in ZM33SA alloy peak-aged at 150 °C at 1000 min and their corresponding FFT shown in inset (**b**) and (**c**).

Furthermore, none of the η' models do not fit with its stacking sequence.

In alloy containing Ag (ZM33SA) in Fig. 3a, c, the plates lying on $\{111\}_{Al}$ planes are 7 layers thick, fully coherent with matrix and with five internal planes with an "a–b" stacking order. Though, the images are a little tilted away from $[110]_{Al}$ zone axis this do not hinder the analyze of precipitates. The central layer shows a subtle contrast compared to the layers positioned at the interface. In addition, from Fig. 3a one can see that five internal planes of $MgZn_2$ can preserve coherency with $\{111\}_{Al}$ planes, till a 6 layer is introduced. In addition, Al atoms may replace in the Zn atom positions in η-$MgZn_2$ [42].

In the present results, η_2 can be well distinguished as seen in Fig. 3a, from its "a–b" layered structure and different interplanar spacing from matrix. Other particle lying on $\{111\}_{Al}$ planes can be assumed η' considering their habit planes, thicknesses and morphologies. In all cases η' and η_2 precipitates incorporate an interface of double layer rich in high-Z atoms. On fast Fourier transformation (FFT) processing of HAADF images of Figs. 2 and 3 are observed diffuse streaks extending toward $[111]_{Al}$ relfections. In consistency with diffuse streaks observed along $[111]_{Al}$ spots in diffraction patterns, indicates that these particles do not have a periodic electron density distribution along their axes parallel with $\langle 111\rangle_{Al}$ direction [6, 43]. This may be due to the fact that as these precipitates are striving to preserve coherency with matrix and as solute atoms have organized into a structure from GP-zones, the internal order is initially not well defined.

η_1 Phase: interface

Figures 4 and 5 show HAADF images of two edge-on particles lying on $\{100\}_{Al}$ planes. Using the matrix and its FFT, calibration of the magnification and measurement on the precipitations were done with respect to the interplanar spacings of Al matrix. The columns in Al matrix are clearly resolved. In this projection from the spots corresponding to the FFT of Al matrix, the separation between neighbor columns is 0.405 nm for $\{100\}_{Al}$ and 0.286 nm for $\{110\}_{Al}$. Due to face-centered cubic crystal structure of Al the nearest neighbor atom columns are shifted by the d-spacing of $\{220\}_{Al}$, 0.143 nm in the viewing direction. In the figure, solid green circles indicate Al atoms lying at the same plane, the open green ones indicate the Al atoms position at ± 0.143 nm displacement normal to the paper plane. Red circles stand for Zn atoms. Exploiting FFT processing of the HAADF images and taking into consideration their habit planes, the following relationships between the precipitates and matrices was found: $(0001)_\eta//(1\bar{1}0)_{Al}$; $(10\bar{1}0)_\eta//(00\bar{1})_{Al}$ corresponding to η_1. The unit cell with reference of η-$MgZn_2$ Komura model is drawn inside the precipitate [21].

Figures 4d and 5d show the magnified sections of the typical interface between η_1 and Al matrix. The zig–zag layer rich in Zn atoms is exposed at the interface in both cases. Such images show the precipitates in which their longest interfaces, corresponding to their c—axis are parallel with $\langle 110\rangle_{Al}$ direction. The unit cell parameter of precipitates can be calculated as three interplanar spacing of $d_{(110)Al}$ which is equal to $c = 0.859$ nm. The full coherency relation along the longest interface is confirmed once more from the FFT processing of HAADF images as shown in Fig. 6. Green circles indicating reflection from $\{220\}_{Al}$ planes will coincide with reflections from $\{0006\}_\eta$ ones. Misfit along $\langle 0001\rangle_\eta//\langle 110\rangle_{Al}$ according to the following equation $[3d_{(110)Al}-d_{(0001)\eta}]/3d_{(110)Al}$ is only 0.34%. Because of coherency, distortion expanding two atomic $d_{\{200\}Al}$ layers away from interface is easily noticed in Figs. 4 and 5. On the other hand, misfit along the short interface is around 9.8% measured from FFT processing (Fig. 6). The simulation of the interface based on both Figs. 4 and 5 using CrystalKitX program is shown in Fig. 7. By comparing simulation with the HAADF images one can see that columns of Zn atoms with higher linear density (shorter periodic repeated distance of

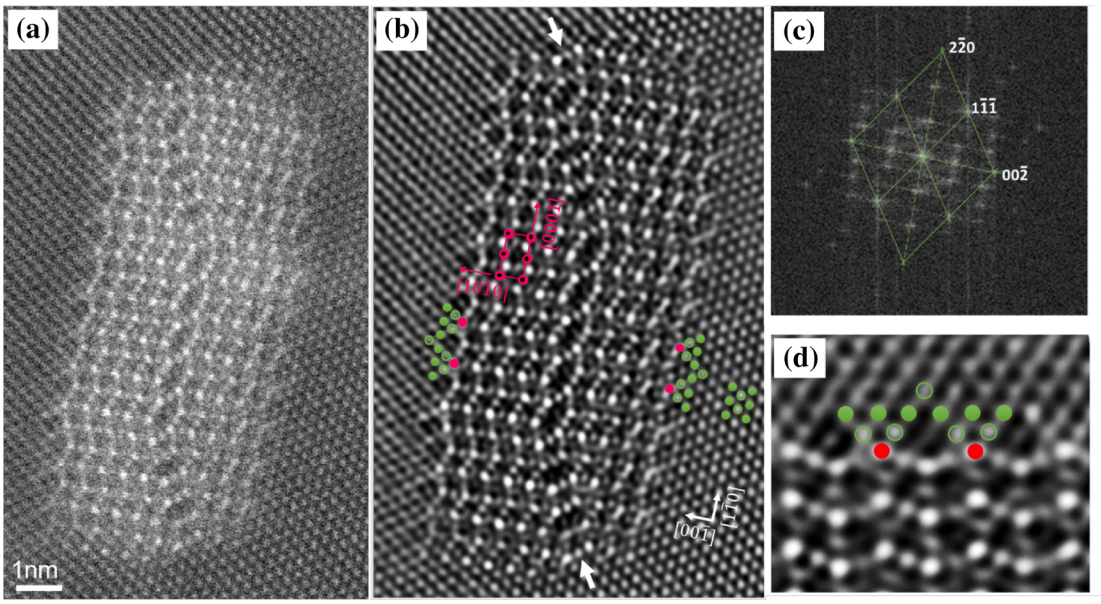

Z (nm)	0	0.143	0	0.133
P (nm)	0.286	0.286	0.257-0.265	0.522
Al				
Zn				

Legend of figure 4 and 5; The height of the atoms normal to paper plane (Z) and periodic repeated distance of atoms parallel with viewing direction (P).

Figure 4 **a** Unprocessed high-angle annular dark field scanning transmission electron microscopy image. **b** Noise suppressed IFFT HAADF image of η_1 under $[110]_{Al}$ projection in ZM33S alloy peak-aged at 150 °C for 1000 min. An internal resembling boundary is indicated with white arrows. Unit cell of $MgZn_2$ phase is overlaid with red color over the precipitate. **c** The Fourier transform of HAADF image of the η_1 embedded in Al. Green lines connect the reflections from Al planes. Other reflections correspond to planes of precipitate. The two diffraction zone axis coinciding are $[110]_{Al}$ and $[\bar{1}2\bar{1}0]_{\eta}$. **d** Magnified section of the interface.

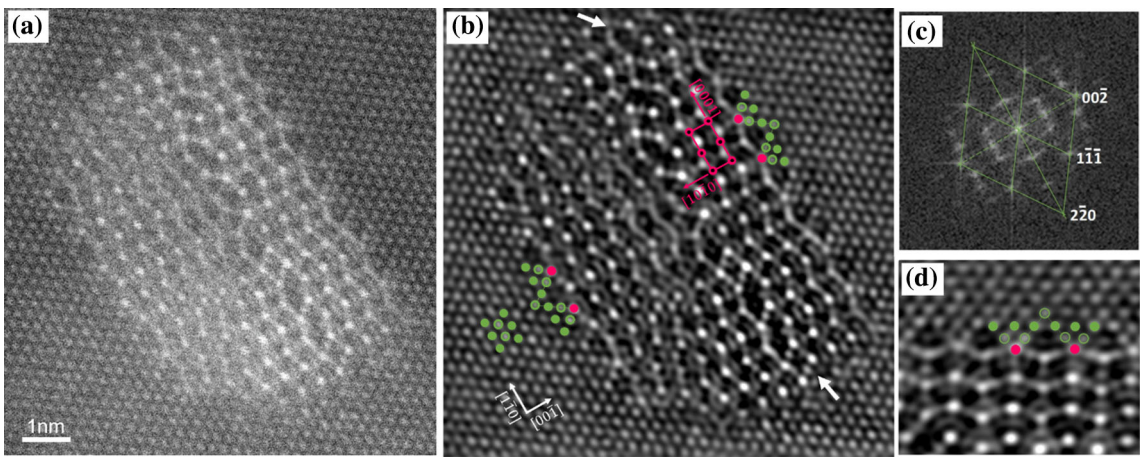

Figure 5 **a** Unprocessed high-angle annular dark field scanning transmission electron microscopy image. **b** Noise suppressed IFFT HAADF image of η_1 under $[110]_{Al}$ projection in ZM33SC alloy peak-aged at 150 °C for 1000 min. An internal resembling boundary is indicated with white arrows. Unit cell of $MgZn_2$ phase is overlaid with red color over the precipitate. **c** The Fourier transform of the HAADF image of the η_1 embedded in Al. Green lines in FFT connect the reflections from Al planes. It confirms that precipitation is under $\langle 110 \rangle_{Al}$ projection. Other reflections are from precipitate's planes. The two diffraction zone axis coinciding is $[110]_{Al}$ and $[\bar{1}2\bar{1}0]_{\eta}$. **d** Magnified section of the interface.

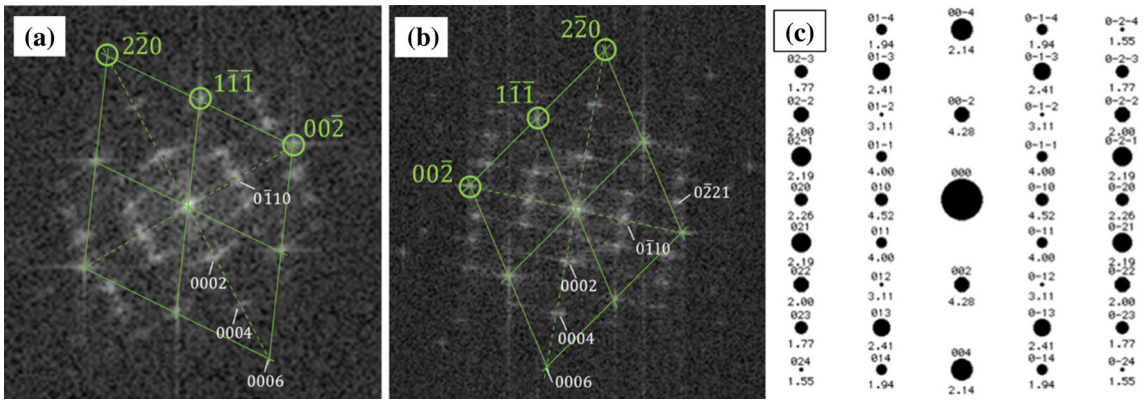

Figure 6 **a**, **b** The Fourier transform of the HAADF images of η_1 phases embedded in Al matrix (respectively of Figs. 4, 5). Simulation of diffraction pattern of η phase under $[\bar{1}2\bar{1}0]_\eta$ with corresponding plane indices and interplanar spacings using MacTempas™ software.

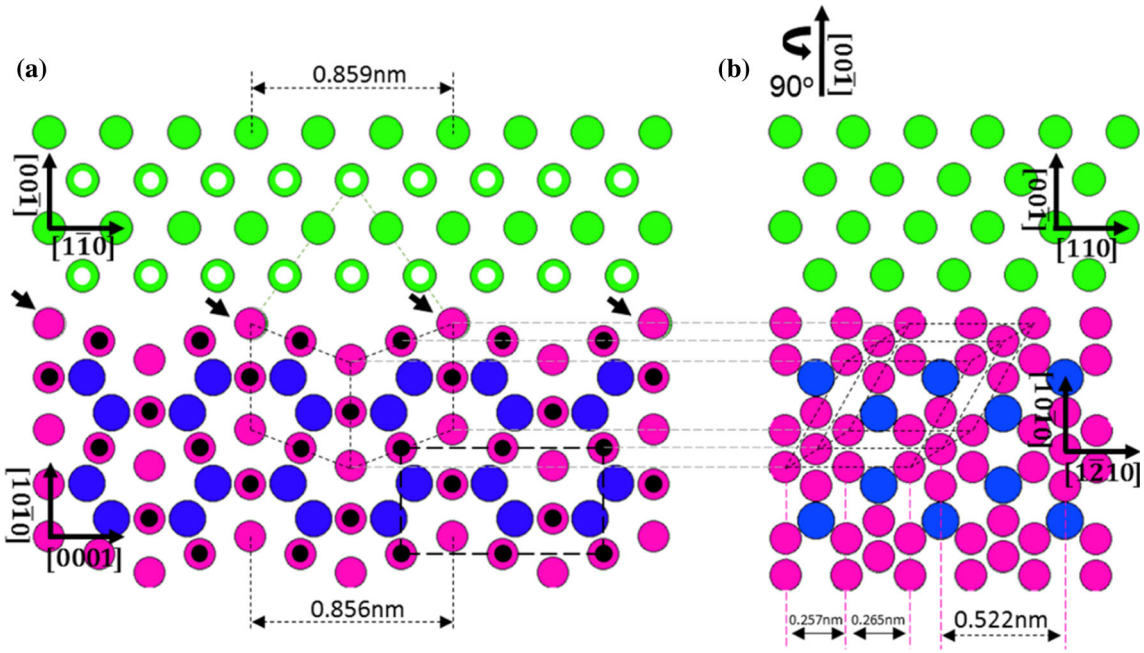

Figure 7 Interface illustration build upon HAADF images of η_1 phase using Komura model ($MgZn_2$) and Al lattice in CrystalKitX **a** interface $\{001\}_{Al}//\{10\bar{1}0\}_\eta$ under coinciding $[110]_{Al}//[1\bar{2}10]_\eta$ zone axis and **b** the same interface under coinciding $[1\bar{1}0]_{Al}//[0001]_\eta$ zone axis (rotated 90°).

atoms, P) will cause brighter contrast. Analyzing the interface with 90° rotation of viewing direction, these atomic columns are highly compacted with respect to matrix than their neighbor ones. Consequently, a high coherency relation or continuity of atomic planes can be excepted between matrix planes periodically spaced with $3d_{\{110\}Al}$ and precipitate planes periodically spaced with $d_{\{0001\}}\eta$ interplanar spacing.

η_1 exposes only one zig–zag interface layer, while coherent precursor η' and η_2 phases expose double layer interface enriched in Zn atoms to the Al matrix. It seems like η'/η_2 phases need an additional interface rich in heavy elements to maintain continuity with closed packed $\{111\}_{Al}$ atomic planes.

η_1 Phase: stacking fault

There are clear stacking faults in the η_1 phase. As a convenient mean for interpreting these stacking faults, visualization of the HAADF images using the rhombic unit cell reference is used in Fig. 8a, b. The net superimposed over precipitation is composed of

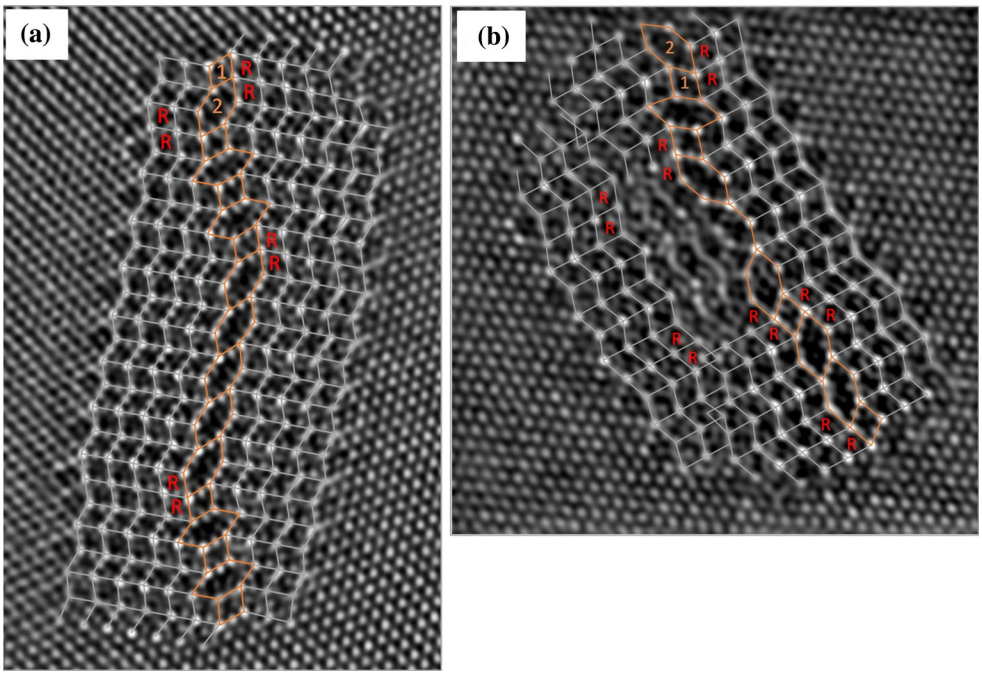

Figure 8 **a**, **b** Visualization of stacking faults that η_1 phase incorporates using orange lines and "R–R" denotation for stacking of rhombic projection unit reference over $MgZn_2$ phase of, respectively, **a** Fig. 4 and **b** Fig. 5 [20]. Bright spots standing at the corners of the rhombic units are atomic columns with shortest periodic repeated distance of Zn atoms.

rhombs, corners of which are columns of Zn atoms with the shortest periodic repeated distance of around 0.261 nm (Fig. 7). These columns will appear with brighter contrast than the adjacent columns of Zn atom with periodic distance of $a = 0.52$ nm.

In the present investigation, it was found that the η_1 precipitate structure is more complex than that of other orientation relationships that η phase creates which Al matrix. There are two atomic arrangements that deviate from the perfect crystal structure of $MgZn_2$. First one labeled "R–R" is formed because of stacking fault of Mg-rich layers along $[0001]_\eta$ direction of η-phase [20]. This stacking fault is commonly observed in all η phases. The other one which was only seen in the orientation relationship of η_1 phases is highlighted with orange color. It lies along the entire length of the particles. These firstly seen disordered regions have a specific structure formed by two atomic arrangements labeled "1" and "2" as seen in Fig. 8.

These anti-phase resembling boundaries separate domains of well-ordered η structure. The way the "1" and "2" atomic arrangements are connected to create this internal boundary indicates also the presence of "R–R" stacking fault. Near this region, the atoms have undergone slight displacements.

Figure 8b shows four domains trapping inside a region clearly absent of Zn atoms. The lack of bright contrast confirms this absence. From subtle contrast of atomic columns, it may be assumed that this precipitate is in the early stages of growth. However, precipitate own structure is clearly noticed. One may assume that Al atoms replace the Zn positions retaining the structure. The same internal boundary is noticed here. It seems like they occur since the very early stages of nucleation.

Inverse FFT of HAAD images shown in Fig. 9 indicates the shift and distortion of planes of precipitates by both types of stacking faults.

Extending lines connecting atoms of the same equivalent planes, a periodic shift was measured in both images over the internal boundary region. Considering the $MgZn_2$ unit cell overlaid with gray lines, this shift is around 0.14 nm. Referring to Al matrix, this value is equal to a Shockley partial which is half of the value of a Burgers vector, $a/2\langle 110\rangle_{Al} = a/6\ \langle 112\rangle_{Al} + a/6\ \langle 112\rangle_{Al}$ as measured under $[110]_{Al}$ zone axis [44]. The shift is indicated with the small gray arrow in Fig. 10a. It seems like the nucleation of this phase happens on a stacking fault, although further investigation is required to clarify this part.

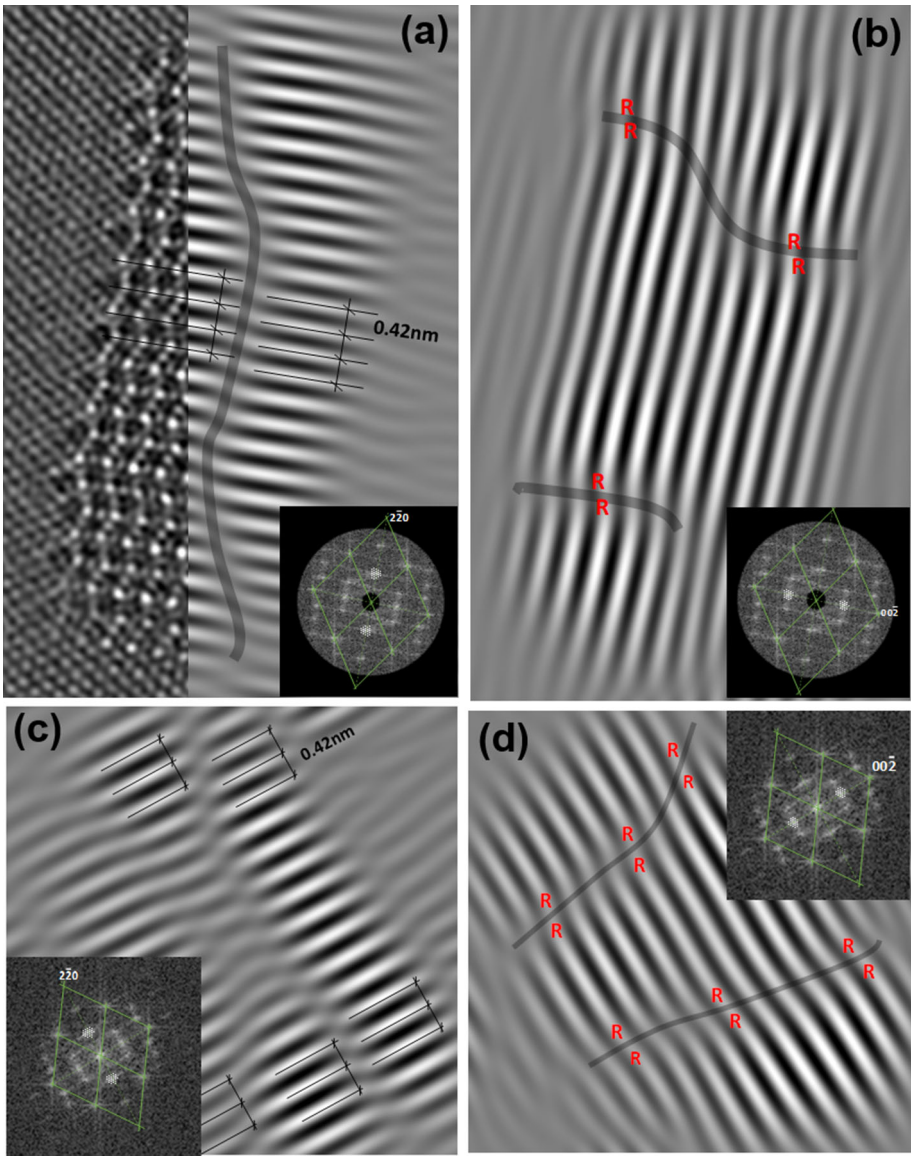

Figure 9 **a**, **c** Inverse of selected reflections from $\{0002\}_\eta$ planes and **b**, **d** from $\{10\bar{1}0\}_\eta$ of the Fourier images. The shift of equivalent planes $\{000l\}_\eta$ with respect to each other over the interconnector region and distortion of $\{h0i0\}_\eta$ because "R–R" stacking fault are clearly seen.

For better characterization, intensity line profiles were obtained from HAAD images as seen in Fig. 10b. Intensities indicate two peaks at the corners of columns of Zn atoms and four low-intensity peaks. Assuming that composition of precipitates should be maintained as $MgZn_2$, these four peaks of low intensity may come from columns of Mg atoms.

Discussion

Most frequently observed precipitates in Al–Zn–Mg(–Cu) alloys are η_1, η'/η_2 and η_4.

η_4 as well as η_5, η_6 and η_7 precipitate heterogeneously as rods or laths on dislocations (Table 3). This requires the samples to be subjected to deformation prior to aging [45].

η'/η_2 Phase

η_2 is formed via a gradual transition from supersaturated solid solution [9]. That requires the sample to be rapidly quenched to room temperature or directly aged below GP-zone solvus in order to be formed in abundance from its precursor η' transition phase. η' has been much debated over its structure throughout years as it was seen by different proposed models. There is a strong similarity between models, and all are strongly connected to structural pattern of equilibrium η-$MgZn_2$ Komura [21]. Wolverton based on

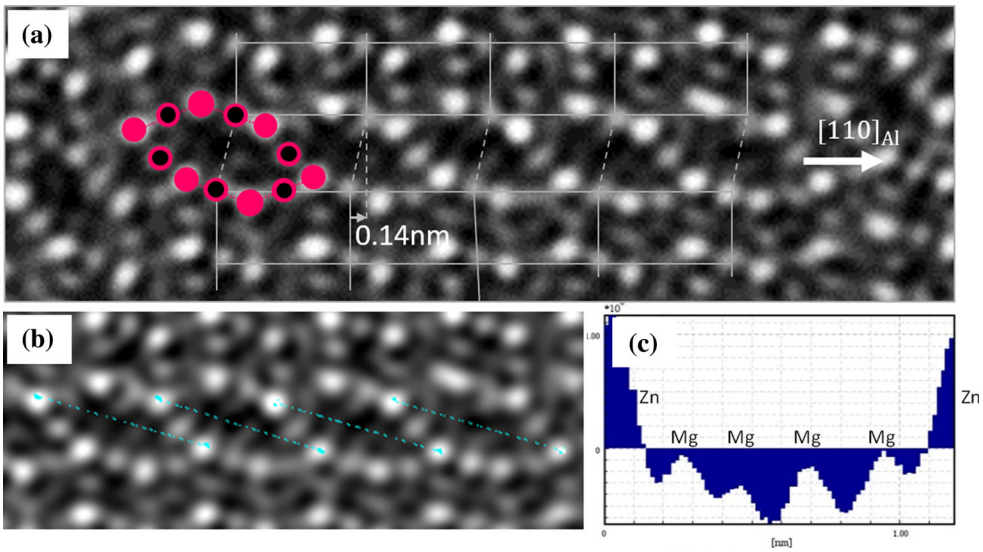

Figure 10 **a** Magnified section of region inside the η_1 phase in which small gray arrow points out the shift equal to $d_{\{220\}Al}$ interplanar spacing parallel with $\langle 110\rangle_{Al}$ matrix. Superimposed unit cell reference of η-$MgZn_2$ Komura model highlighted with gray lines, **b** line profile edge to edge of interconnector showing, **c** high-intensity peak corresponding to columns of Zn atoms and four low-intensity peaks.

first principle energy calculations concluded that from η' models of Gjonnes and Simensen [12], Auld and Cousland [14] and Li et al. [18] the most energetically favorable was that of Auld and Cousland [46]. Comparing Auld model and internal structure of Marioara Type 1 shows a striking match [14, 20]. Models indicate that the central layer composed of Al atoms in Auld model may be substituted by Mg ones as seen in the centered layer in O-unit of Marioara Type 1 model. In addition, Auld reported the stringing similarity between its structure and equilibrium η-$MgZn_2$. "F" sites in his η' model occupied by Zn atoms are occupied by Mg atoms in η-$MgZn_2$ structure [14]. The only difference being the lattice parameters and centered layer of Al atoms can be considered as coincident with sites of the surrounding solid solution [14].

The present investigation is supported by the results of Li [37] and Marioara [20] for striking similarities that η' phase has with η-$MgZn_2$ equilibrium one.

However, in present results, it was seen that particles can grow to 13 layers thick, without transforming to equilibrium η phase. This is in contradiction with the proposed idea that 11 layers thick is the smallest entity that can be associated with the η phase [37]. One can assume that Cu may modify the misfit of interface, rendering easier for precipitate to retain coherent relation with the matrix.

In Ag-added alloy particles were 7 layers thick, with five internal layers. From the observed particle in Fig. 3a it was seen that five internal planes of $MgZn_2$ can preserve coherency with $\{111\}_{Al}$ planes, till a 6 layer is introduced.

This means that five internal layers of $MgZn_2$ gripped from two interfacial layers can maintain coherency with $\{111\}_{Al}$ planes.

Excluding the precipitate shown Fig. 3b which deviates from the "a–b" stacking sequence, in all other cases the particles were build up from "a–b" stacking sequence where "a" Zn-rich planes and "b" Al-/Mg-rich ones corresponding to the building layers of $MgZn_2$ [21, 38].

η_1 Phase

η_1 nucleation conditions are unclear. It is assumed that η_1 is nucleated directly on GP-zones when aging below GP-zone solvus [32]. Others concluded that η_1 particles are directly nucleated from the solid solution due to the fact that they were numerous in samples directly or slowly quenched to aging temperatures above 150 °C [12, 23, 24]. Precipitation directly from the solid solution is supported by the fact that η_1 volume fraction increases when aging is carried out above around 150 °C. 130–160 °C is the temperature range in which the GP-zone solvus lye for Al alloys with solute content ranging for Zn from 4 to 6 wt% and Mg from 1 to 3 wt% [5, 27, 32, 33, 47]. 155 °C is the temperature that changes the dispersion of precipitates by a factor of about 1000 in a temperature range of 10 °C for Al matrix containing 5.9 wt% Zn and 2.9 wt% Mg [48]. In light of the present investigation, the fact that equilibrium phase

can maintain coherency with matrix by orientating its $\{10\bar{1}0\}_{\eta}$ plane parallel with elastically soft $\{100\}_{Al}$ plane is a strong reason to believe that the nucleation of this phase does not need a transitional phase with higher coherency with Al matrix in which to nucleate.

But the reason why it needs a high aging temperature to increase its precipitated volume fraction in Al matrix requires further investigation.

The size of η_1 is about two times that of η'/η_2 for the same aging time, temperature and alloy composition. This means that η_1 had either nucleated earlier or the precipitate growth speed had been higher.

Such kind of morphologies of precipitates grow in larger thicknesses of by ledge mechanism. After the solute atoms will accumulate in interface, enriching $\{100\}_{Al}$ planes, the collapse of a region of these layers enriched in solute atoms creating a unit more thickness of precipitate will cause an immediate collapse of adjacent solute-enriched Al layers [49].

Conclusions

The microstructure of Al–Zn–Mg alloy peak-aged at 150 °C for 1000 min after water quenching was investigated using atomic scale HAADF-STEM characterization. The plates lying on $\{111\}_{Al}$ and $\{100\}_{Al}$ planes were the most commonly found in our alloy peak-aged at 150 °C for 1000 min. The orientation relationships of these plates were mostly that of η'/η_2 and η_1, although η_3 and η_9 were also observed lying on $\{111\}_{Al}$ and $\{100\}_{Al}$ planes. Moreover, it was observed that the particles habiting $\{111\}_{Al}$ planes can grow to 13 layers thick without transforming to η_2 phase. Retainment of coherency or not may be a strong classifying criterion between η'-$MgZn_2$ and η-$MgZn_2$.

Analyzation of observed η_1 phase was done.

While η'/η_2 phases have interfaces composed of double layers rich in high atomic number elements, η_1 has only one zig–zag layer rich in Zn atoms. As a plate-like shape particle, it has a long and full coherent interface with Al matrix, where matrix planes periodically spaced with $3d_{\{110\}Al}$ interplanar spacing have continuity with precipitate planes periodically spaced with $d_{\{0001\}\eta}$ interplanar spacing. Comparing to η'/η_2 phase, η_1 overall structure consists of ordered domains that are separated by anti-phase resembling boundaries. The structure of these boundaries is determined by the shift of atomic planes with an distance of about $d_{\{220\}Al}$, or 0.14 nm. This region was not observed to be part of other precipitates.

Acknowledgements

This work was supported by JST (Japan Science and Technology Agency) under collaborative research based on industrial demand "Heterogeneous Structure Control": Toward innovative development of metallic structural materials. The authors also acknowledge Dr. Junya Nakamura, Mr. Ryoma Arita and Prof. emeritus Susumu Ikeno, University of Toyama. A part of this research was supported by President description, University of Toyama (2017).

References

[1] Starke EA Jr, Staley JT (1996) Application of modern aluminum alloys to aircraft. Prog Aerosp Sci 32:131–172

[2] Berg LK, Gjonnes J, Hansen V, Li XZ, Knutson-Wedel M, Waterloo G, Schryvers D, Wallenberg LR (2001) GP-zones in Al–Zn–Mg alloys and their role in artificial ageing. Acta Mater 49:3443–3451

[3] Guinier A (1952) Interprétation de la Diffusione Anormale des Rayons X pas les Alliages à Durcissement Structural. Acta Cryst 5:121–130

[4] Matsuda K, Kawai A, Watanabe K, Lee S, Marioara CD, Wenner S, Nishmura K, Matsuzaki T, Nunomura N, Sato T, Holmestad R, Ikeno S (2017) Extra electron diffraction spots caused by fine precipitates formed at the early stage of ageing in Al–Mg–X (X = Si, Ge, Zn)—Cu Alloys. Mater Trans 58(2):167–175

[5] Jiang X, Noble B, Holme B, Waterloo G, Tafto J (2000) Differential scanning calorimetry and electron diffraction investigation on low-temperature aging in Al–Zn–Mg alloys. Metall Mater Trans A 13A:339–348

[6] Sha G, Cerezo A (2004) Early-stage precipitation in Al–Zn–Mg–Cu alloy (7050). Acta Mater 52:4503–4516

[7] Engdahl T, Hansen V, Warren PJ, Stiller K (2002) Investigation of fine scale precipitates in Al–Zn–Mg alloys after various heat treatment. Mater Sci Eng A 327:59–64

[8] Stiller K, Warren PJ, Hansen V, Angenete J, Gjonnes J (1999) Investigation of precipitation in an Al–Zn–Mg alloy after two-step ageing treatment at 100° and 150°C. Mater Sci Eng A 270:55–63

[9] Park JK, Ardell AJ (1983) Microstructures of the commercial 7075 Al alloy in the T651 and T7 tempers. Metall Trans A 14A:1957–1965

[10] Mondolfo LF, Gjostein NA, Levinson DW (1956) Structural changes during the aging in an Al–Mg–Zn alloy. Trans AIME J Metals 8:1378–1385

[11] Graf R (1957) Comptes rendus hebdomadaires des séances de Académie des sciences, Paris: 244

[12] Gjonnes J, Simensen CJ (1970) An electron microscope investigation of the microstructure in an Aluminum–Zinc–Magnesium alloy. Acta Metall 18:881–890

[13] Auld JH, Cousland SM (1971) The transition phase η' in Al–Zn–Mg alloys. Scr Metall 5:765–770

[14] Auld JH, Cousland SM (1974) The structure of the metastable η' phase in Aluminium–Zinc–Magnesium Alloys. J Aust Inst Metals 19:194–199

[15] Mondolfo LF (1976) Aluminum alloys: structures and properties. Butterworths, London

[16] Régnier PC, Bouvaist J, Simon JP (1982) Etude Cristallographique de la Phase de Transition M' dans Al-8%Zn-1%Mg. J Appl Cryst 15:590–593

[17] Auld JH, Cousland SM (1985) On the structure of the M' phase in Al–Zn–Mg alloys. J Appl Cryst 18:47–48

[18] Li XZ, Hansen V, Gjonnes J, Wallenberg LR (1999) H.R.E.M study. Acta Mater 47:2651–2659

[19] Kverneland A, Hansen V, Vincent R, Gjonnes K, Gjonnes J (2006) Ultramicroscopy 106:492–502

[20] Marioara CD, Lefebre W, Andersen SJ, Friis J (2013) Atomic structure of hardening precipitates in an Al–Mg–Zn–Cu alloy determined by HAADF-STEM and first principle calculations: relation to η—$MgZn_2$. J Mater Sci 48:3638–3651

[21] Komura Y, Tokunaga K (1980) Structural studies of stacking variants in Mg-base Friauf–Laves phases. Acta Cryst B36:1548–1554

[22] De Ardo AJ, Simensen CJ (1973) A structural investigation of multiple aging of Al—7 wt pct Zn—2.3 wt pct Mg. Metall Trans 4:2413–2421

[23] Ryum N (1975) Precipitation Kinetics in an Al–Zn–Mg-Alloy. Z Metallkde 66(6):338–343

[24] Thackery PA (1968) The nature and morphology of precipitate in Al–Zn–Mg alloys. J Inst Metals 96:228–237

[25] Godard D, Archambault P, Aeby-Gautier E, Lapasset G (2002) Precipitation sequences during quenching of the AA710 alloy. Acta Mater 50:2319–2329

[26] Bergman G, Waugh JLT, Pauling L (1957) The crystal structure of the metallic phase Mg32(Al, Zn)49. Acta Cryst 10:254–258

[27] Cornish AJ, Day MKB (1971) The effect of variable quenching conditions on the relationship between the stress–corrosion–resistance, tensile properties, and micro-structure of a high-purity Al–Zn–Mg alloy. J Inst Metals 99:377–384

[28] Par M. Bernole et R. Graf (1972) Influence du zinc sur la decomposition de la solution solide sursaturee Al–Mg. Memoires Scientifiques Rev. Metallurg., LXIX, N.2, pp 123–142

[29] Marlaud T, Deschamps A, Bley F, Lefebre W, Baroux B (2010) Influence of alloy composition and heat treatment on precipitate composition in Al–Zn–Mg-Cu alloys. Acta Mater 58:248–260

[30] Polmear IJ (1960) The ageing characteristics of complex Al–Zn–Mg alloys. Distinctive effects of copper and silver on the ageing mechanism. Inst Metals 89:51–59

[31] Chinh NQ, Lendvai J, Ping DH, Hono K (2004) The effect of Cu on mechanical and precipitation properties of Al–Zn–Mg alloys. J Alloy Compd 378:52–60

[32] Parker BA (1972) The effect of certain trace element additions on the ageing behavior of an Aluminum-4 wt% Zinc-3 wt% Magnesium alloy. J Aust Inst Metals 17(1):31–38

[33] Zahra A, Zahra CY, Lacom W, Degischer HP (1982) Comments on "the influence of Mg contents on the formation and reversion of Guinier–Preston zones in Al-4.5at%Zn-xMg alloys". Z Metallkde 3068–3071

[34] Watanabe K, Matsuda K, Ikeno S, Yoshida T, Murakami S (2015) TEM observation of precipitate structures in Al–Zn–Mg alloys with additions of Cu/Ag. Arch Metall Mater 60:977–979

[35] Pennycook SJ, Nellist PD (2011) Scanning transmission electron microscopy: imaging and analysis. Springer, New York

[36] Maloney SK, Hono K, Polmear IJ, Ringer SP (2001) The effects of trace addition of silver upon elevated temperature ageing of an Al–Zn–Mg alloy. Micron 32:741–747

[37] Li Y-Y, Kovarik L, Phillips PJ, Hsu Y-F, Wang W-H, Mills MJ (2012) High-resolution characterization of the precipitation behavior of an Al-Zn-Mg-Cu alloy. Philo Mag Letters 92(4):166–178

[38] Stein F, Palm M, Sauthoff G (2004) Structure and stability of Laves phases. Part I. Critical assessment of factors controlling Laves phase stability. Intermetallics 12:713–720

[39] Ohba T, Kitano Y, Komura Y (1984) The charge-density study of the laves phases, $MgZn_2$ and $MgCu_2$. Acta Cryst C40:1–5

[40] Ying XR, Du YX, Song M, Lu N, Ye HQ (2016) Direct measurement of precipitate induced strain in an Al–Zn–Mg–Cu alloy with aberration corrected transmission electron microscopy. Micron 90:18–22

[41] Wenner S, Friis J, Marioara CD, Holmestad R (2016) Precipitation in a mixed Al–Cu–Mg/Al–Zn–Mg alloy system. J Alloy Compd 684:195–200

[42] Fang X, Song M, Li K, Yound D, Zhao D, Jiang C, Zhang H (2012) Effects of Cu and Al on the crystal structure and composition of η ($MgZn_2$) phase in over-aged Al–Zn–Mg–Cu alloys. J Mater Sci 47:5419–5427

[43] Martin JW (1998) Precipitation hardening, 2nd edn. Butterworth Heinemann, Oxford

[44] Dieter GE (1961) Mechanical metallurgy, 2nd edn. MCGraw-Hill, New York

[45] Allen RM, Vander Sande JB (1980) The oriented growth of precipitates on dislocations in Al–Zn–Mg part I. Experimental observations. Acta Metall 28:1185–1195

[46] Wolverton C (2001) Crystal structure and stability of complex precipitate phases in Al–Cu–Mg–(Si) and Al–Zn–Mg alloys. Acta Mater 49:3129–3142

[47] Inoue H, Sato T, Kojima Y, Takahashi T (1981) The temperature limit for GP zone formation in an Al–Zn–Mg alloy. Metall Trans A 12A:1429–1434

[48] Embury JD, Nicholson RB (1965) The nucleation of precipitates: the system Al–Zn–Mg. Acta Metall 13:403–417

[49] Porter DA, Easterling KE (1992) Phase transformations in metals and alloys, 2nd edn. Chapman & Hall, London